Removal rates for the collisional quenching of various vibronic levels of ground state NCO by simple molecules (N_2, O_2, NO, CO_2, N_2O, and SO_2)

José A. Fernández, Pilar Puyuelo, David Husain,[a] María N. Sánchez Rayo, and Fernando Castaño[b]
Departmento de Química Física, Universidad del País Vasco, Apartado 644, 48080 Bilbao, Spain

(Received 27 September 1997; accepted 27 January 1997)

The collisional behavior of NCO[$\tilde{X}(0,n,0)$] in specific vibronic states in the gas phase has been investigated in the time-domain by laser-induced fluorescence (LIF) on transitions within the system NCO($\tilde{A}\ ^2\Sigma^+ - \tilde{X}\ ^2\Pi$). The NCO radical was generated by the infrared multiphoton dissociation (IRMPD) of phenyl isocyanate (PhNCO) by means of a TEA-CO_2 laser operating on the 9R24 line at $\lambda = 9.25\ \mu$m with subsequent monitoring of the vibronic levels of the $\tilde{X}$ state, characterized by Renner–Teller coupling, in the presence of N_2, O_2, NO, CO_2, N_2O, SO_2, and PhNCO itself. The states probed were as follows: $(00^10)^2\Pi_{3/2}$, $(00^10)^2\Pi_{1/2}$, $(01^00)\mu^2\Sigma^+$, $(01^20)^2\Delta_{5/2}$, $(01^20)^2\Delta_{3/2}$, $(02^10)\mu^2\Pi_{3/2,1/2}$, $(02^30)^2\Phi_{7/2}$, and $(02^30)^2\Phi_{5/2}$. Various pairs of spin–orbit states were found to be tightly coupled kinetically. Thus, the time-evolution of the pairs of vibronic states $(00^10)^2\Pi_{3/2}$ and $(00^10)^2\Pi_{1/2}$; $(01^20)^2\Delta_{5/2}$ and $(01^20)^2\Delta_{3/2}$; $(02^30)^2\Phi_{7/2}$ and $(02^30)^2\Phi_{5/2}$ were found to be equal, yielding an effective local equilibrium within these spin–orbit components within experimental error. Further, states such as NCO(01^00) and NCO(01^20) were characterized by relatively long decay profiles in the presence of molecules such as CO_2 and O_2 where the contribution of rotational quenching to the overall decay process could be neglected. By contrast, NCO(02^10) and NCO(02^30) were removed on significantly faster time scales on collision with SO_2. In the absence of extensive information required for solving the large set of coupled differential kinetic equations, albeit reduced in number of those states strongly coupled kinetically, such as a detailed knowledge of the nascent state distributions in NCO following IRMPD, not necessarily Boltzmann in character, the vibronic states were taken to behave independently as the most practical approach to this study. Absolute second-order rate data for the collisional quenching of NCO in the vibronic states (00^10), (01^00), (01^20), (02^10), and (02^30) by the above molecular species are reported. No clear selection rules are apparent except for the low propensity rule $\Delta K = 2$ within the same vibronic state, i.e., $\mu\ ^2\Sigma^+(01^00) - ^2\Delta_{5/2}(01^20)$ and $^2\Pi_{3/2,1/2}(02^10) - ^2\Phi_{7/2}(02^30)$. This is presumed to reflect the role in the collisional interaction of the oscillating dipole in the vibronic state, facilitating $\Delta K = 1$, whereas $\Delta K = 2$ would involve the quadrupole which is smaller. It is found that the data for $(V-V)$ and $(V-T)$ energy transfer correlate best with the attractive part of the potential curves between the collision partners using the established Parmenter–Seaver plots, yielding well depths $[(\epsilon_{MM}/k_B)^{1/2}]$ for the vibronic states NCO[$\mu\ ^2\Sigma^+(01^00)$, $^2\Delta_{5/2}(01^20)$, $^2\Pi_{3/2,1/2}(02^10)$, and $^2\Phi_{7/2}(02^30)$], significantly larger than those of the closed shell collision partners and equal within experimental error. The data are also considered in terms of a multipolar attractive force model involving a collision complex where a sensible correlation is found between the computed and observed collision cross sections for O_2, N_2, CO_2, N_2O, and SO_2 assuming no change in the multipoles with vibrational state. © *1997 American Institute of Physics.* [S0021-9606(97)02417-3]

I. INTRODUCTION

The role of symmetry in collisional quenching processes is a fundamental subject in chemical dynamics and has been extensively investigated for electronic states for both light and heavy species.[1,2] Adiabatic correlation rules combining states of defined atomic and the molecular symmetry have been derived by Wigner and Witmer,[3] and, more recently, correlation rules have been extended to the reactions of polyatomic systems in the weak spin–orbit coupling approximation[2(a)] and in (J,Ω) coupling.[2(b)] For triatomic and higher polyatomic molecules, the level of symmetry approximation has necessarily needed to be simplified both in terms of the geometry in the collision and the associated ''least symmetrical complex'' and also the Hund's coupling cases employed.[1,2] Direct experimental investigations on the role of symmetry on collisions of species in specific, accessible, molecular vibronic states has necessarily been limited.

The species selected for the study of the influence of molecular vibronic symmetry on collisional relaxation

[a]Permanent address: Department of Chemistry, University of Cambridge, Lensfield Road, Cambridge CB2 1EW, England.
[b]Author to whom correspondence should be addressed; fax: 34-4-464-8500; electronic mail: qfpcaalf@lg.ehu.es

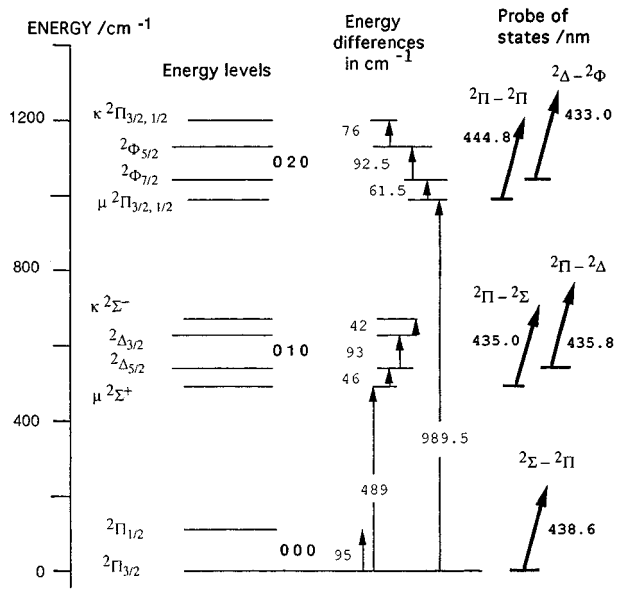

FIG. 1. Schematic diagram of the vibronic energy levels and symmetry states within the electronic ground state of NCO. The energy differences between selected levels within the same vibrational state and between vibrational states are indicated. Information on some of the transitions used to probe the relative population of the vibronic states by LIF following IRMPD of PhNCO are also included. More detailed wavelength assignments are presented in Table I.

properties in the present investigation is the fragment, NCO, a 15 electron open shell linear molecule with the following low lying X, A, and B electronic states: ,$\ldots(1\pi)^4(\sigma)^2(2\pi)^3X(^2\Pi_i)$,$\ldots(1\pi)^4(\sigma)(2\pi)^4A(^2\Sigma)$ and $\ldots(1\pi)^3(\sigma)^2(2\pi)^4B(^2\Pi)$.[4,5] Linear NCO belongs to the $C_{\infty v}$ symmetry group and, because the external atoms, N and O in the molecular structure have similar masses, the normal vibrational modes are closely described by a near symmetric stretch, $v_1(\Sigma^+)$, an asymmetric vibration, $v_3(\Sigma^+)$, and a doubly degenerate bending mode, $v_2(\Pi)$. In the degenerate vibration, angular momentum along the molecular axis, is of magnitude $l_i\mathbf{h}(l_ih/2\pi)$, where $l_i = v_i, v_{i-2}, \ldots$, 1 or 0 ($v_i$ is the degenerate vibrational quantum number), and contributes to the vibrational energy term-values via anharmonic terms.[4] This vibrational angular momentum couples with the electronic angular momentum, Λ, in the open shell, yielding the vibronic angular momentum, K, whose quantum numbers are determined as $K = |\pm l \pm \Lambda|$.[5] The magnitude of this interaction and the subsequent splitting is measured by the so-called Renner expansion parameter, ϵ, and the effect results in a classic breakdown of the Born–Oppenheimer adiabatic approximation known as the Renner–Teller effect.[6] Spin–orbit coupling, of course, also contributes to split the quantum levels further, where, for example, the degenerate $^2\Pi$ ground electronic state splits into the $\Omega = 1/2$ and 3/2 fine-structure components and the other states couple with this accordingly, resulting in a pattern of energies schematized in Fig. 1. In addition to the Renner–Teller effect and spin–orbit coupling, molecular states of NCO are also influenced by Fermi-resonance between the vibrations $2v_2$ and v_1. Figure 1 thus summarizes the main features of the spectroscopy of this molecule, including the nomenclature of the vibronic levels within the overall ground state electronic structure, and the electronic transitions used to probe these levels by laser-induced fluorescences.

The rich spectroscopy of NCO was first reported in the classic studies by Dixon[7,8] who measured the emission spectra of the $A-X$ and the $B-X$ band systems and presented an approximate set of spectroscopic constants and a Renner coupling parameter. Following the EPR detection of the ground states $(000)^2\Pi_{3/2}$, $(010)^2\Delta_{5/2}$, and $(020)^2\Phi_{7/2}$ (Fig. 1) by Carrington *et al.*,[9] Bolman *et al.*[10] obtained higher resolution spectra associated with the bending hot band (010), and, as a consequence, were able to improve the earlier values of the spectroscopic constants, the Renner parameter, ϵ, and to characterize the energy levels of the Σ and Δ vibronic states in more detail. Later, Woodward *et al.*[11,12] detected fluorescence to vibronic levels of Π symmetry associated with the Fermi-resonant pair of levels (020) and (100), leading to the determination of the interaction parameters. The rotational structure of the vibronic levels (000), (010) and $(020)^2\Phi$ has been characterized to high accuracy by microwave spectroscopy. The quartic and sextic centrifugal distortion constants, the lambda doubling parameter, q, and various g factors were determined by mid-infrared laser magnetic resonance (LMR) and diode laser absorption spectroscopy.[13–15] More recently, spectroscopic investigations on higher lying vibronic levels of the ground state have been reported by several research groups,[16–21] and, as a consequence, a considerable number of the energy levels in this molecule have become particularly well established.

Vibrational relaxation of this triatomic open-shell species has been little studied although considerable attention has been directed towards rotational relaxation, particularly in accounting for the lambda doublet propensity rules in the $^2\Pi$ electronic states.[22] It has been suggested that this occurs via nonadiabatic deactivation processes.[23–26] The first determination of collisional quenching rate constants for the bending vibrational levels in NCO(X) by the series of rare gases and by NO has been reported recently.[27,28] Rate data were reported for NCO in the vibration levels $(010)^2\Delta$ and $(020)^2\Phi$, and, in contrast to vibrational quenching of closed-shell molecules (CO_2, OCS, NO_2, etc.),[29–36] the observed trend for these noble gases was not that expected on the bases of either the Schwartz–Slawsky–Herzfeld (SSH)[37,38] or the vibrational close coupling infinite order adiabatic approximation theories.[39–41] In consequence, a nonadiabatic mechanism has been proposed to account for the results.[27] The evolution of the low lying vibrational states $(010)^2\Sigma$ and the $(020)^2\Pi$ were found to be those of $^2\Delta$ and $^2\Phi$, respectively. Molecular beam experiments of the scattering of vibrationally energized NCO with He has shown that the population of the (01^20) vibronic manifold is not in direct proportion with the initial $(01^00)\mu^2\Sigma$ population, but to other vibronic states, implying a intervibrational mixing comparable to other collisional processes reported in this system.[42] Implications for the collisional rotational relaxation with He and Ar have also been reported.[43–45]

The kinetic behavior of ground NCO, a crucial intermediate in the combustion of the nitrogen-containing organic molecules, has attracted considerable attention. Reactions with H_2, O_2, NO, NO_2, H_2CO, hydrocarbons, alkanes, etc. across a broad range of temperature have been studied in depth.[46–53] In this paper, collisional removal rates of the population of five accessible vibronic states of the electronic ground state of NCO, eight states considering the similar behavior of close lying states, are reported for singlet, doublet, and triplet stable reactant molecules. The paper is constructed in the following way. Section II gives a concise summary of the experimental details, including the description of the preparation and identification of the NCO vibronic states. Section III describes in a systematic way the interpretation of the results. Finally, in Sec. IV the results and discussed within the context of various empirical theories.

II. EXPERIMENT

The experimental arrangement used to generate NCO by infrared multiphoton photodissociation (IRMPD) and to monitor state selected populations of this molecule by laser-induced fluorescence (LIF), thus permitting the determination of collisional removal rates for these states, is analogous to that described previously for the study of the fragments CHF and CFCl (Refs. 54–58) and will only be briefly summarized here. The pulsed photodissociation of phenyl isocyanate, henceforth PhNCO, was effected by means of a TEA-CO_2 laser (Lumonics K-103) operating on the 9R24 line at $\lambda = 9.25\ \mu$m. The laser pulse consisted of a spike of ~ 100 ns duration followed by a long ($\sim 3\ \mu$s), low-intensity, tail containing approximately half of the laser output energy. The beam was focused using a 2 in. silicon lens to a spot of average diameter 1.5 mm in the center of a stainless steel sample cell. The average fluences employed varied in the range from 80 to 43 (36) $J\ cm^{-2}$ using appropriate attenuaters though these values should only be taken as relative averaged fluences when considering the determination of a rate constant at threshold, when a fluence dependence was found, as the laser spot size is not precisely characterized in each instance. The sample cell was filled with the precursor PhNCO (8.0 mTorr; 1 Torr$=133.32\ N\ m^{-2}$), buffer gas (Ar, 1.0 Torr) and the selected reactant partner at variable pressures (usually in a range up to 250 mTorr). The precursor pressure selected represented a compromise between obtaining sizable laser-induced fluorescence emission signals and a low noise background due to luminescence caused either by collisional dissociation of the precursor molecules following infrared laser multiple photon absorption or by reaction and energy transfer of MPD transients with or without added reactant gases.

State selected NCO$[\widetilde{X}(0,n,0)]$ was probed in the time-domain by a Nd:YAG/dye coupled system (Quantel 581 and Datachrom) using cumarin 440 and 450 dyes to scan the region from 432 to 450 nm, where the NCO$[A-\widetilde{X}(0,n,0)]$ transitions of interest are located.[7–21] Spectra were recorded with a variable delay between the photodissociation and probe lasers of 0.2, 2 μs, and 10–40 μs. The laser resolution used either for static or time resolved measurements was $\Delta\lambda = 0.16\ cm^{-1}$. Crossed laser beams were used to improve the luminescence signal to noise level. The kinetic behavior of several vibronic levels of the electronic $\widetilde{X}$ state was monitored by varying the delay of the photolysis and probe lasers and by measuring the time-dependent fluorescence signals directly with a fast side-on photomultiplier (Hamamatsu R928) connected to a digital oscilloscope (Tektronix TDS 520) IEEE interfaced with a PC-computer. Time-resolved removal rates were obtained by nonlinear fitting. In all cases, care was taken in the subtraction of background luminescence signals. For experiments using standard mixtures of the photochemical precursor, the buffer gas and the selected quenching partner at predetermined pressures as measured with a capacitance manometer (Datametrics 10–0.001 Torr), these were prepared in a spherical bulb using magnetic stirring for a minimum of 30 min before flowing into the reaction vessel. Once in the reaction vessel, NCO was produced by IRMPD of the precursor and the vibronic populations followed by LIF.

All experiments were carried out at room temperature (~ 295 K). Chemicals used were PhNCO (>99.0 vol %, Fluka), Ar (99.9995%, SEO), N_2 (99.999%, ArgonSA), O_2 (99.99%, SEO), NO (99.0%, Matheson), NO_2 (99.0%, ArgonSA), N_2O (99.5%, ArgonSA), and SO_2 (99.98%, ArgonSA). PhNCO, NO, NO_2, SO_2, and N_2O were subject to freeze–pump–thaw cycles in a separate vacuum manifold to remove impurities. O_2 and N_2 were used as commercially available. Commercial laser dyes (Exciton) were used throughout.

Preparation and identification of fragments. An example of the NCO($\widetilde{A}\ ^2\Sigma^+ - \widetilde{X}\ ^2\Pi$) LIF spectrum generated by the high intensity IRMPD of the precursor PhNCO in argon (10 mTorr/1 Torr) at room temperature and a 25 μs delay between the dissociation and probe lasers, at wavelengths in the range from 432 and 449 nm is depicted in Fig. 2. The emission bands of this spectrum are readily assigned to the $\widetilde{A}-\widetilde{X}$ transition of the NCO transient[7–21] with no interferences by emission from other transient species created by IRMPD, including that of cyclopentadienyl nitrile, recently identified in this type of system.[59,60] The clear separation of the transitions allows the collisional decay within the specific vibrational states to be studied. The wavelengths of transitions used to probe the various states studied are presented in Table I some of which are shown schematically in Fig. 1.

The selection of conditions favorable for the efficient production of NCO in specific vibrational states, required for characterizing rate data for these states, was determined by empirical observation. For most dissociation processes using IRMPD, it is normally assumed that the resulting nascent population distribution in the photodissociation fragments is Boltzmann in character, however, this is not necessarily observed in this system. The presence of argon buffer gas strongly influences the initial relative populations of ground and vibrational states of the NCO created in the IRMPD process. The production of NCO(000) and NCO(01^10) at

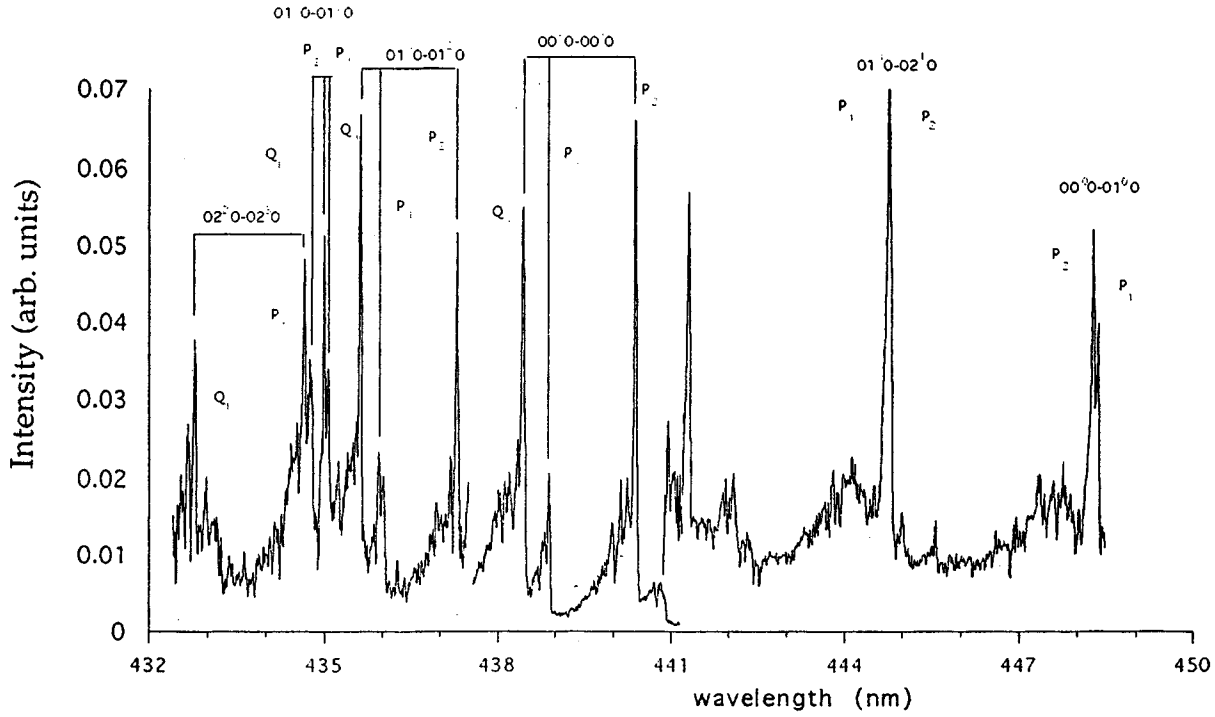

FIG. 2. Laser-induced fluorescence spectrum of the $A-X$ transition of the NCO fragment generated by the IRMPD of PhNCO. [p(PhNCO)=10 mTorr; p(Ar)=1 Torr.] The delay between the dissociation and probe lasers was 25 μs. The wavelengths correspond to those read directly from the laser meter, shifted 0.12 nm to the blue with respect to the absolute values of Patel-Misra *et al.* (Refs. 18,19).

high laser fluence (80 J/cm^2) has been observed to be small at low argon pressure, increasing by a factor of $\sim$3 at pressures of 2–3 Torr and laser decreasing slowly and steadily for pressures up to 10 Torr. However, the NCO(02^10) level is relatively more efficiently produced at low buffer pressures. The threshold fluorescence intensity also increases with the energy of the vibrational state, as shown in Fig. 3, with a relationship closely exponential in character. The pressure of the precursor also plays an important role in this initial vibrational distribution. For pressures higher than 4 mTorr, the appearance of NCO(000) increases very rapidly with pressure (Fig. 4). The NCO(010) and NCO(020) populations show a steady, fluence dependent, increase with the precursor pressure up to 60 m Torr, suggesting the use of precursor pressures in the range 10–20 mTorr for studies of vibrationally excited states.

TABLE I. Tunable laser wavelengths used to probe the (000), (010), and (020) vibrational states of NCO in the time domain. The transitions marked with an asterisk * overlap with other bands or are not clearly distinguished and were not probed.

Transition	Branch	Wavelength (nm)
$(01^10)^2\Sigma^+\leftarrow(00^10)^2\Pi_{3/2}$	Q_1	438.60
$(00^00)^2\Sigma^+\leftarrow(00^10)^2\Pi_{1/2}$	P_2	440.48
$(01^10)^2\Pi\leftarrow(01^00)\mu^2\Sigma^+$	P_2	434.99
$(01^10)^2\Pi\leftarrow(01^20)^2\Delta_{5/2}$	Q_1	435.78
$(01^10)^2\Pi\leftarrow(01^20)^2\Delta_{3/2}$	P_2	437.62
$(01^10)^2\Pi\leftarrow(01^00)\kappa^2\Sigma^-$	not observed	*
$(01^10)^2\Pi\leftarrow(02^10)\mu^2\Pi_{3/2,1/2}$	P_1,P_2	444.76
$(02^20)^2\Delta\leftarrow(02^30)^2\Phi_{7/2}$	Q_1	432.97
$(02^20)^2\Delta\leftarrow(02^30)^2\Phi_{5/2}$	P_2	434.77
$(01^10)^2\Delta(b)\leftarrow(02^10)\kappa^2\Pi_{3/2,1/2}$	overlapped	435.87*

The translational temperature was determined by the method of King,[61–67] yielding values close to ambient conditions (250 ± 50 K). As with studies on other triatomic species,[54,58] this determination may be taken as a rough indication of the final temperature at longer times in the decay processes. Unfortunately, one is unable to make a sensible estimate of the rotational temperature on the basis of spectra similar to that shown in Fig. 3. It may be argued from the geometry of PhCNO, with a major axis along the NCO fragment, that, on photodissociation, the rotational temperature should be small (400 K). Similarly, an equilibrium procedure could not be employed to determine the vibrational temperature as the LIF method is not sufficiently sensitive for accurate intensity measurements across a range of vibrational states in order to characterize the vibrational energy distribution.[54] Finally, in terms of nascent populations, we may note the effect of laser fluence on the relative intensity of the LIF products, examples of which are shown in Fig. 4 for various vibronic states of NCO. After threshold, the relationship is essentially linear and consistent with the foregoing observations on the role of energy absorption and of the pressure employed.

III. INTERPRETATION OF LIF PROFILES

The time-evolution of the population of a specific vibronic state ideally requires the solution of a set of coupled

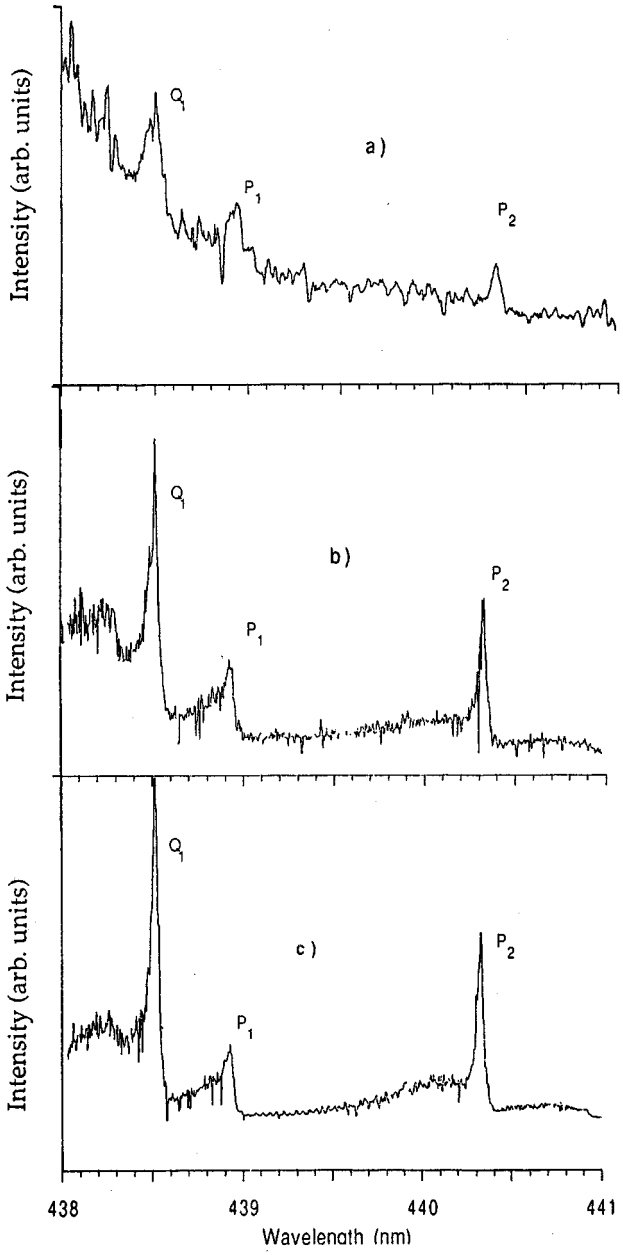

FIG. 3. Rotational relaxation of NCO demonstrated in the LIF band system $A(000)\leftarrow\tilde{X}(00^10)$ following the IRMPD of PhNCO in the presence of Ar. p(PhNCO)=10 mTorr PhNCO; p(Ar)=500 mTorr Ar; CO_2-laser fluence =80 J/cm^2. Delay between dissociation and probe lasers (a) 0.2 μs; (b) 2.0 μs; (c) 40 μs.

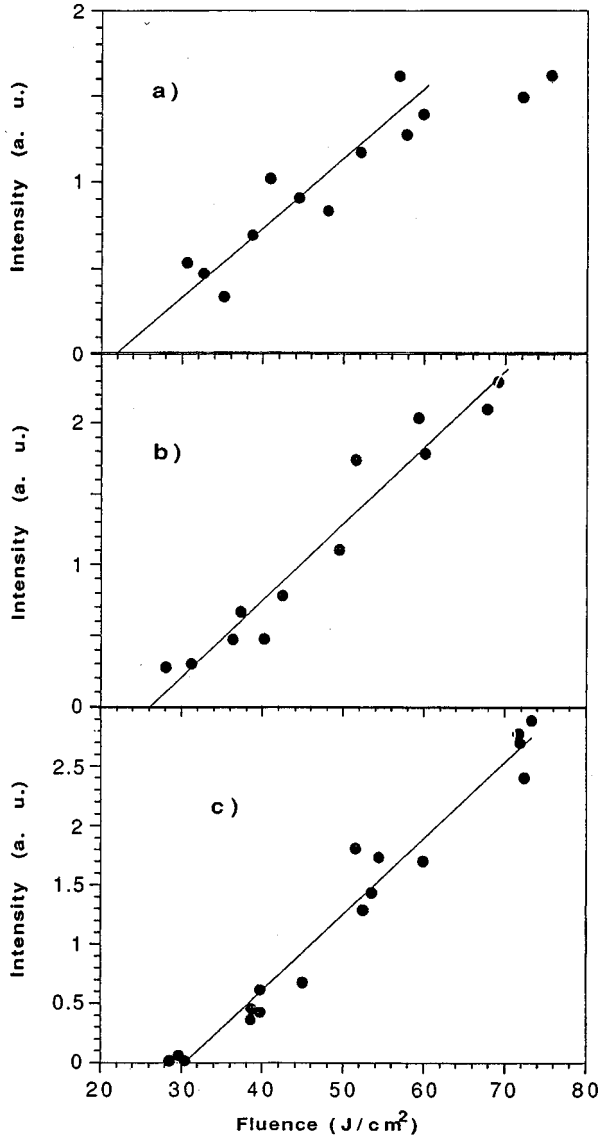

FIG. 4. Intensity of the LIF spectra of some vibronic state of the NCO fragment generated by the IRMPD of PhNCO as a function of the CO_2-laser fluence (a) NCO $(000)^2\Pi_{1/2}$; (b) NCO $(01^20)^2\Delta_{3/2}$; (c) NCO $(02^30)^2\Phi_{7/2}$.

kinetic differential equations for all the degenerate and close lying states in the vibronic manifold. However, this task is reduced by comparing the decay profiles of a number of observable transitions that probe specific states and which are tightly coupled due to factors such as being close lying and effectively providing a local equilibrium (Table I). Indeed, the time evolution of the population of the vibronic states $(00^10)^2\Pi_{3/2}$ and $(00^10)^2\Pi_{1/2}$; $(01^20)^2\Delta_{5/2}$ and $(01^20)^2\Delta_{3/2}$, and $(02^30)^2\Phi_{7/2}$ and $(02^30)^2\Phi_{5/2}$, probed at the wavelengths shown in Table I, have been found to be consistently equal, within only small marginal differences, the first pair demonstrating this equality by inspection of the profiles. This observation reduces the number of kinetically independent states and implies the existence a fast collisional mechanism that equilibrates the population of species within the same vibrational state but where the total angular momentum differs by one unit (fine structure component $\Delta\Omega=1$). Within the same vibrational state, the decays of the populations of the $(01^00)\mu^2\Sigma^+$ and $(01^20)^2\Delta_{5/2}$ states, and those of the $(02^10)\mu^2\Pi_{3/2,1/2}$ and $(02^30)^2\Phi_{7/2}$ states show small but consistent differences. The latter states have vibronic angular momentum differences of $\Delta K=2$ and, in spite of the quasiresonance (Fig. 1), the population equilibration is less efficiently achieved than by quenching with the series of molecules studied, which are themselves of lower efficiency. Considering the differences that are observed for

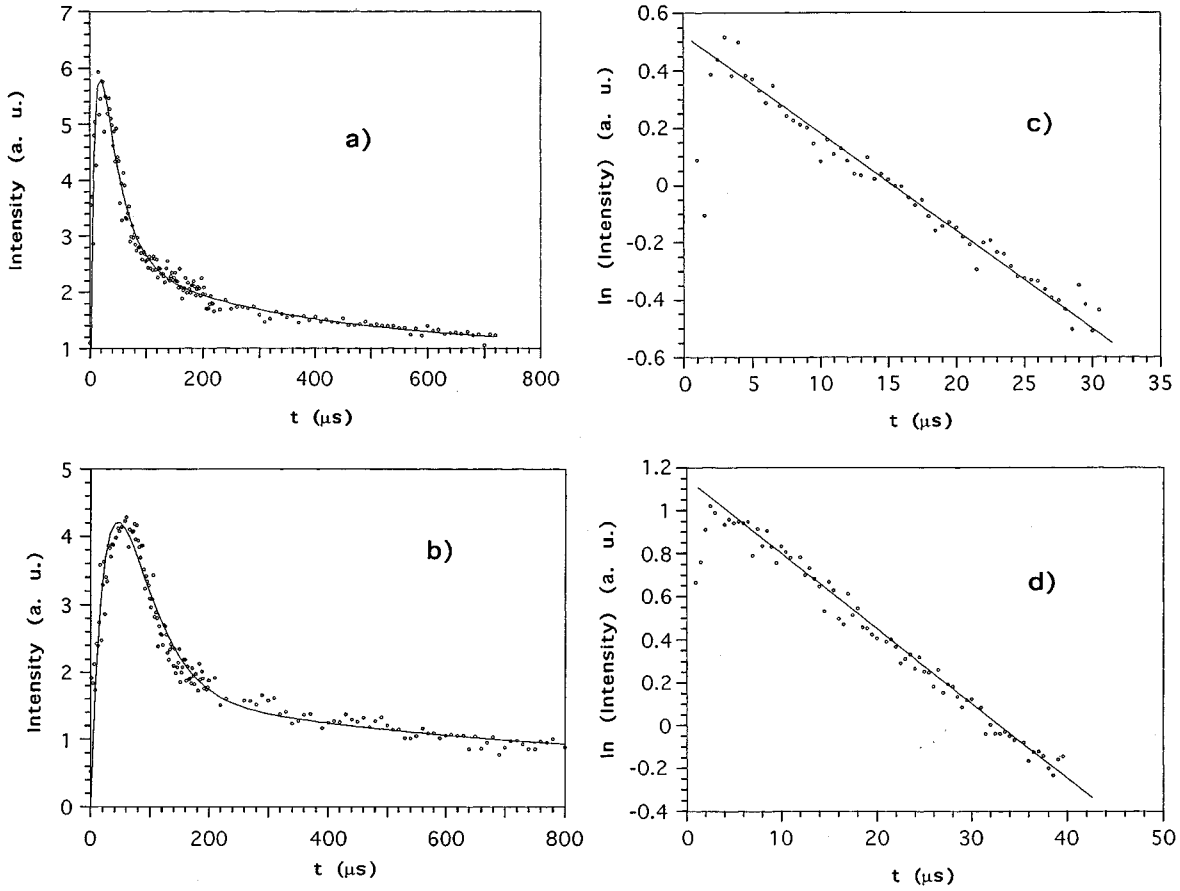

FIG. 5. Examples of LIF profiles indicating differing decay plots for the removal of NCO in different vibronic states in the presence of various simple molecules. [p(PhNCO)=8 mTorr, p(Ar)=1 Torr.] (a) NCO ($\tilde{X}(01^{0}0)+CO_2$: $p(CO_2)$=120 mTorr; (b) NCO ($01^{2}0)+O_2$: $p(O_2)$=52 mTorr; (c) NCO ($02^{1}0)+SO_2$: $p(SO_2)$=160 mTorr; (d) NCO ($02^{3}0)+SO_2$: $p(SO_2)$=160 mTorr. For the states within (010) the continuous curve describes the nonlinear best fit to a sum of a growth profile and exponential components for collisional quenching and diffusional loss (see text).

slow and fast quenching species, it can be concluded that the multiplet mixing for $\Delta K=2$ is of relatively low efficiency and provides a propensity rule. Higher levels of these vibrational states $\{(01^{0}0)\kappa^{2}\Sigma^{-}$ and $(02^{1}0)\mu^{2}\Pi_{3/2,1/2}\}$ could not be monitored separately, nevertheless, on the basis of observations described for multiplet mixing, it can be stated that population interchange with states closest in energy, where $\Delta K=2$, is expected to be relatively low in efficiency. On the other hand, the energy difference with the parental low state is of the order of 181 and 230 cm^{-1}, spacings comparable to those of the translational energies, and twice the difference between the Δ and Φ states where mixing is shown to be very fast on the time scales for quenching, so that these energy transfer processes should be rapid on the time scales considered here.

Profiles of selective vibrational states always show the same pattern of behaviour, namely, an increase in the population in the first $\sim$0.4 μs followed by a rapid exponential decay that finally leads to a slow diffusional component. As can be appreciated from examples of the type shown in Fig. 3, the rotational population is high at short times, decreasing rapidly with time when the corresponding vibrational state acts as a sink for rotational energy.[61–67] A quantitative description of the time-profiles for the various selected state populations based on the overlap the two Gaussian dissociation and monitoring laser pulses is complex and an averaged effective empirical quenching parameter is used as an appropriate fit to the experimental results. The empirical equation employed for growth component is given by

$$n_i=n_{i0}(1-e^{-\lambda t}),$$

where n_{i0} is the population of state i for the temperature of dissociation and λ has a value of the order of 3×10^{5} s^{-1}. Figure 5 shows the population history of some selected excited states and their fit to the above equation to the growth component at short times and an exponential profile of the type $n_{i0}e^{-kt}$ at longer times. The central portion of the population profile contains the information of the decay rate of the specific state of interest. In the case of the two states, $(02^{1}0)\mu^{2}\Pi_{3/2,1/2}$ and the $(02^{3}0)^{2}\Phi_{7/2}$, the contribution by diffusion to the overall first-order decay coefficient is negligible which can thus be written as

$$k=\{k_0+k_1[\mathrm{PhNCO}]+k_2[\mathrm{Ar}]\}+k_3[Q]=k'+k_3[Q],$$

where Q is the added quenching gas, k_1 and k_2 are defined for the appropriate gases in the overall first-order decay coefficient, and k_0 represents the contribution by all other loss processes.

Figures 5(a) and 5(b) show examples of first-order decay profiles in this central region for the quenching of the NCO(01^00) and NCO(01^20) states in the presence of CO_2 and O_2, respectively, where rotational quenching has been neglected. These states demonstrate relatively slow quenching rates and the contribution by diffusional loss must be included. Two methods were employed to include this. The first employs the ''long-time'' solution of the diffusion equation, involving the appropriate geometry of the system, and which subsequently involves diffusional loss by a first-order contribution to the overall first-order decay coefficient (k) for the appropriate species, and whose magnitude which is inversely proportional to pressure.[68] Consequently, k can be written as

$$k = k' + k_3[Q] + \beta'/P_{\mathrm{Ar}},$$

where β' includes the appropriate diffusion coefficient and the geometrical boundary conditions of the system. Fittings of the decay profiles using this method were poor in spite of earlier successes employing this approach in emission studies on electronically excited alkaline earth atoms using one laser only for initial excitation.[69,70] In the second approach diffusion is assumed to be independent and for the two perpendicular beam lasers and, at a total pressure of about 1 Torr, the integrated contribution to diffusional loss is given by

$$S(t) = S_0 b (b + c^2 t^2)^{-1},$$

where S_0 and b are components contributing to the signal at zero time, and include factors proportional to the sum of the squared beam diameter and to the most probable velocity.[64] As some of these quantities are not clearly defined in the measurements, particularly overlapping of the laser beam diameters, they were taken as empirical fitting parameters. Examples of fitting profiles with the slower quenching processes including contributions from growth, quenching by the added reactant partner and empirical correction to diffusional loss as described above are given as the full curves in Figs. 5(a) and 5(b). For rapid decay profiles, plots of the type given in Figs. 5(c) and 5(d) for NCO(02^10) and NCO(02^30) with SO_2, neglecting diffusion loss, were employed to obtain collisional rate data. For processes characterised by less efficient collisional quenching and where the diffusional contribution must be included, overall decay coefficients for quenching were analysed using the second of the two procedures described above with the appropriate quenching gases and with pressures varying up to 250 mTorr. These were then employed using the standard Stern–Volmer-type relationship to obtain the absolute second-order rate constants. Figure 6(a) depicts examples of such Stern–Volmer plots of the pseudo-first-order rate coefficients for removal of NCO($\tilde{X}(01^00)$ and NCO($\tilde{X}(02^10)$ with the slowest quenching gas, N_2, on the one hand, and Fig. 6(b) that for NCO($\tilde{X}(01^00)$ and NCO($\tilde{X}(01^20)$ with the faster quenching gas, SO_2, on the other.

Finally, in this context, we may emphasize the need to employ the present approach with that of the most general quantitative approach of solving the coupled linear kinetic

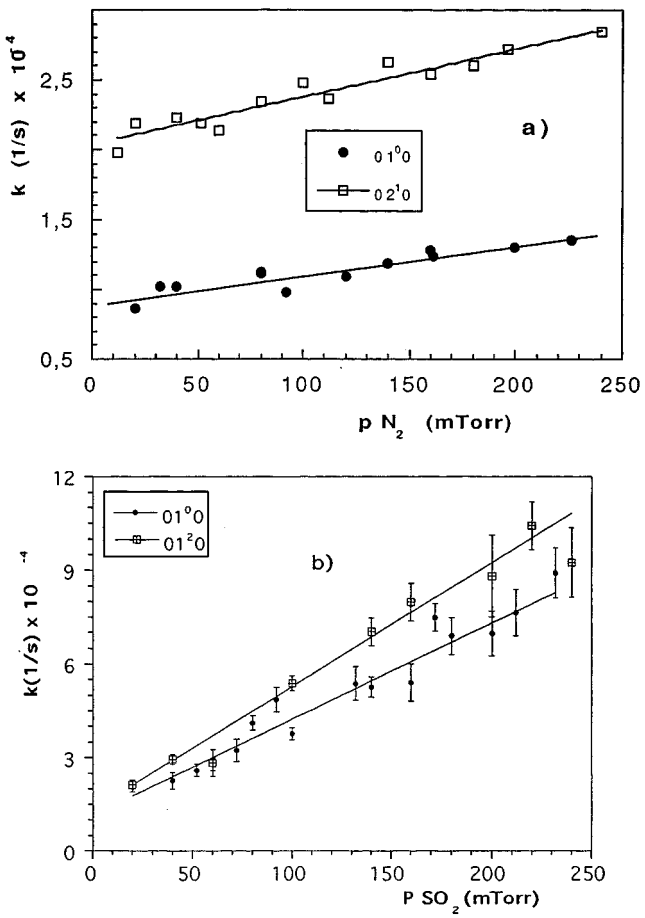

FIG. 6. Examples of the variation of the pseudo-first-order rate coefficients $[k(1/s)]$ for the collisional quenching of vibronically excited NCO following the IRMPD of PhNCO in the presence of N_2 and SO_2. (a) NCO in the states $\tilde{X}(01^00)$ and $\tilde{X}(02^10)$) with N_2. (b) NCO in the states $\tilde{X}(01^00)$ and $\tilde{X}(01^20)$) with SO_2.

equations for the evolution of the population of the range of states investigated here. The number of equations can be reduced where states are coupled strongly kinetically as seen from experimental observations of the time-evolution of the states $^2\Pi_{1/2}$ and $^2\Pi_{3/2}$ of the vibrational level (000) as well as others states involving processes where ΔK was the same and which were concluded to be characterized by having the same decay constants. Even with this simplification, and restricting the analysis to five independent NCO state populations, by themselves involving a considerable number of rate constants for fitting, it would still be necessary to make assumptions concerning, for example, nascent populations on photodissociation, as we have seen, not necessarily described by a Boltzmann distribution. Apart from the vibronic lifetimes which are the object of the kinetic measurements, the diffusion equation would need to be coupled fully to the coupled kinetic equations as well as employing the principle of detailed balance for all pairs of states kinetically linked. From the foregoing, it can be seen that the most appropriate approach is that employed here, namely, to characterize the effective decay coefficients for each state where the major and necessary approximation is the assumption of indepen-

TABLE II. Rate constants (room temp) in units of 10^{-12} cm^3 molecules^{-1} s^{-1} for the quenching of NCO in the vibronic states (00^10), (01^00), (01^20), (02^10), and (02^30). Note that states split by spin–orbit coupling, e.g., (01^20), $^2\Delta_{3/2}$, and $^2\Delta_{5/2}$, show the same experimental decay constant. The indicated errors correspond to 1σ taken from the best fit.

	00^10	01^00	01^20	02^10	02^30
N_2	< 0.01	0.82 ± 0.10	0.85 ± 0.1	1.1 ± 0.1	1.8 ± 0.3
N_2O	< 0.01	2.9 ± 0.3	4.9 ± 0.5	5.3 ± 0.5	6.3 ± 0.5
NO	32.0 ± 3.0		37.0 ± 2.0		57.0 ± 6.0
	31.8 ± 2.3 (Ref. 46)				
	34.0 ± 3.0 (Ref. 28)				
	34.0 (Ref. 47)				
	37.9 (Ref. 71)				
	40.3 (Ref. 72)				
	33.5 (Ref. 73)				
O_2	< 0.01	1.64 ± 0.13	1.2 ± 0.3	2.2 ± 0.2	3.6 ± 0.2
CO_2	< 0.01	3.5 ± 0.3	5.0 ± 0.4	4.8 ± 0.2	5.3 ± 0.4
SO_2	< 0.01	9.5 ± 0.7	12.3 ± 0.6	10.9 ± 0.4	12.9 ± 0.6
PhNCO	1.11 ± 0.16[a]				
	1.04 ± 0.17[b]				
	0.80 ± 0.18[c]				

[a]Fluence 80 J/cm^2.
[b]Fluence 60 J/cm^2.
[c]Fluence 43 J/cm^2.

dent behaviour of the vibronic states, such as neglecting the effect of cascading from higher states in measurements of the decay profiles, apart from those tightly linked by rapid energy transfer and characterized by the same decay coefficients.

IV. RESULTS AND DISCUSSION

Ar buffer is known to influence the nascent distribution of vibrational and rotational states of IRMPD products. Unfortunately, apart from direct experimental observations of the type described in this paper, relatively little is known fundamentally and quantitatively of the varied processes involved and how to control them. In the range of pressures and pulse energies employed here, no significant variations in the relative populations were seen for the various vibronic states selected for measurements. A significant conclusion of the present investigation is to note that vibronic states with the same K quantum numbers (Fig. 1) are characterized by identical rate constants. In contrast energy transfer between vibronic states involving a difference of $\Delta K = 2$ show different quenching rate constants and also show definite trends in kinetic behavior for different quenching gases and for the various vibronic states. This applies to collision partners in either singlet or triplet (O_2) states. This is direct experimental evidence of the low efficiency of a collisional propensity rule where $\Delta K = 2$.

The precursor PhNCO is expected to quench vibrationally excited states of NCO efficiently. Since PhNCO dissociates by IR absorption, it is clear that increasing the absorbed IR radiation will result in an increase in the internal vibrational state distribution and hence the observed quenching rate constants should be a function of laser fluence. Interference by fluorescence restricted determination of the rate constants for quenching by the precursor to the ground state. For fluences of 43, 60, and 80 J/cm^2, these were found to be $0.80 \pm 0.18 \times 10^{-12}$, $1.04 \pm 0.17 \times 10^{-12}$, and $1.11 \pm 0.16 \times 10^{-12}$ cm^3 molecules^{-1} s^{-1}, respectively (Table II).

Table II lists the rate constants for room temperature obtained by the present direct method, including data calculated from Arrhenius forms.[71–73] The quoted errors, restricted here to 1σ, reflect both the experimental error in the data in each case and, equally important in our view, an analysis necessarily based on independent collisional behavior of each vibronic level as indicated in Sec. III. The diatomic molecules $N_2(^1\Sigma)$ and $O_2(^3\Sigma)$ quench the vibronic states of NCO with different efficiencies. The overall pattern of the behavior is as follows, namely, higher removal rates for higher vibrational states and, within the same vibrational state, a faster rate is observed for the higher energy state. The triatomic SO_2 is the only simple nonlinear molecule used as quenching species in this study, demonstrating a quenching rate a factor of ~ 10 greater than that of the inert molecule, N_2, which clearly involves no chemical interaction on collision. The relative errors in the two sets of data for SO_2 and N_2 are, of course, similar. The vibrational modes of SO_2 overlap very closely with those of NCO in either the (010) and (020) states and highly efficient $V-V$ transfer rates are expected. Figure 6(b) shows the Stern–Volmer plot of the rate coefficients for the NCO states $^2\Delta_{5/2}$ and $\mu^2\Sigma^+$ as obtained by the present method for a number of samples with SO_2 at pressures up to 250 mTorr. Absolute collisional quenching rate constants derived from the slopes of the straight lines from these plots together with those for the two (020) vibronic states studied with this molecule are collected in Table II. Similarly, kinetic studies have been carried out for collisional quenching of the same set of vibronic states of NCO with the linear molecules N_2O and CO_2 and the resulting second-order rate constants are also listed in Table II.

A number of conclusions can be drawn from observation of the absolute rate constants collected in Table II. Rate constants for collisional quenching of any of the vibronic states of NCO increase in the series $N_2<O_2<CO_2\approx N_2O<SO_2(<PhNCO<NO)$. For any of the quenching gases, the rate constants increase with the energy and follows the series $^2\Pi(000) \ll \mu\ ^2\Sigma^+(01^00) < {}^2\Delta_{5/2}(01^20) < {}^2\Pi_{3/2,5/2}(02^10) < {}^2\Phi_{7/2}(02^30)$. No clear correlation rules are apparent except for the low propensity rule $\Delta K = 2$ within the same vibrational state, i.e., $\mu\ ^2\Sigma^+(01^00)-{}^2\Delta_{5/2}(01^20)$ and $^2\Pi_{3/2,5/2}(02^10)-{}^2\Phi_{7/2}(02^30)$. This could reflect the role in the collision of the oscillating dipole in the vibronic states, facilitating processes involving $\Delta K=1$, whereas $\Delta K=2$ would involve the quadrupole which would be smaller.

Whilst one can present the thermochemistry for the removal of NCO by the simple molecules whose collisional quenching is investigated here (Table II) for a range of overall processes, these are mainly endothermic for fundamental reactions and it is not particularly helpful to describe them all. Attention here is restricted to the reactions between NCO+NO as these have been considered by Perry,[46]

	ΔH/kJ mol^{-1}
$NCO+NO\rightarrow N_2O+CO$	-278
$NCO+NO\rightarrow N_2+O+CO$	-109
$NCO+NO\rightarrow N_2+CO_2$	$-640.$

It would appear that NO reacts chemically with NCO though the detailed products are not clear. PhNCO is also very efficient at quenching but no attempt been made to identify the products of reaction which is clearly a complex matter. The other quenching gases possess vibrational modes very close to those of the spacings (000)–(010), (010)–(020) and also (000)–(020) in NCO. It is instructive to consider the correlation between the quenching cross section (σ) and the closest NCO-quenching partner resonance (ΔE) as shown in Fig. 7 in the form $\log_{10}(\sigma)$vs the magnitude of this energy discrepancy for $V-V$ transfer. As expected, significant differences are observed for collisional quenching of the (010) and (020) vibronic states as seen from the general form of the data in Fig. 7 where differences can be seen for quenching involving these two vibrational levels. The relationship between $\log(\sigma)$ and ΔE when considered in linear form for collisional processes involving near resonance partners for $V-V$ energy transfer is close to that expected and it may be concluded that SO_2 and N_2O deactivate any of the vibronic states with a mechanism of this type. For collision partners involving nonresonant processes, a plot constructed on the same basis [$\log(\sigma)$ vs ΔE] would normally exhibit smaller cross sections for large ΔE, indicating the role of $V-T$ energy transfer which would include, for example, the effect of the relative masses of CO_2, O_2, and N_2 in terms of a distorted wave model based on a mechanism of the type described by Schwarz, Slawsky, and Herzfeld.[37,38] However, it must be noted that the SSH model[37,38] is strongly influenced by the role of the translational matrix element on the repulsive component of the interaction potential, usually derived from Lennard-Jones parameters.

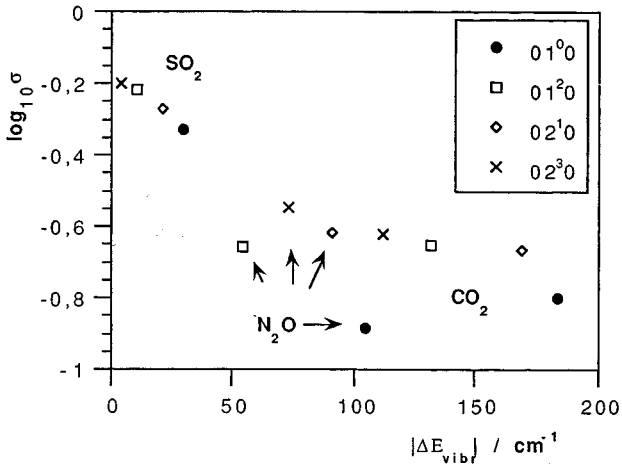

FIG. 7. Relationship between the decimal logarithm of the collisional quenching cross section (σ/Å^2) of low vibronic states of NCO and the energy difference (ΔE_{vib}) for ($V-V$) energy transfer for the molecular partners SO_2, N_2O, and CO_2. Only the closest transitions to the NCO $\Delta K=\Delta J=1$ are considered. For SO_2, where less interference from other partner transitions are found, a linear correlation is found. NCO transitions with $\Delta K=1$, $\Delta J=2$; $\Delta K=2$, $\Delta J=2$, etc. appear to show a lower $V-V$ energy transfer efficiency.

The processes of vibrational–vibrational and vibrational–translational energy transfer, in fact, correlates with the attractive part of the potential curves between the partners of the quenching process.[74] Parmenter and Seaver suggest a correlation between the logarithm of the collision cross sections, σ, with the well depth of the reactants,[74,75] according to the equation

$$\ln \sigma = \ln C' + \beta(\epsilon_{MM}/k_B)^{1/2},$$

where C' is a constant and ϵ_{MM} is the potential well depth for two identical quenching species, M. The slope β depends exclusively on the vibronic state of the NCO itself and is given by the expression

$$\beta = (\epsilon_{MM}/k_B T^2)^{1/2},$$

where ϵ_{MM} represents the potential well depth of two identical vibronic NCO fragments. The removal rates obtained in this investigation for those vibronic states and collision partners studied to date are presented in Fig. 8 in this form excluding the results for NO (Table III). It should be noted that, with the exception of quenching by NO for the different vibronic levels, a clear correlation of this type exists for all the partners studied, with no major differences arising from the symmetry of the ground state collision partner. It is well known from observations on product formation and commented on in this paper, that NO reacts chemically with NCO, a process very different from those of the other collision partners and consequently, different behavior in context of Fig. 8 may be expected.

It can be broadly concluded that the magnitude of the attractive well depths involved in the $V-V$ and the $V-T$ energy transfer processes are of similar order. From the

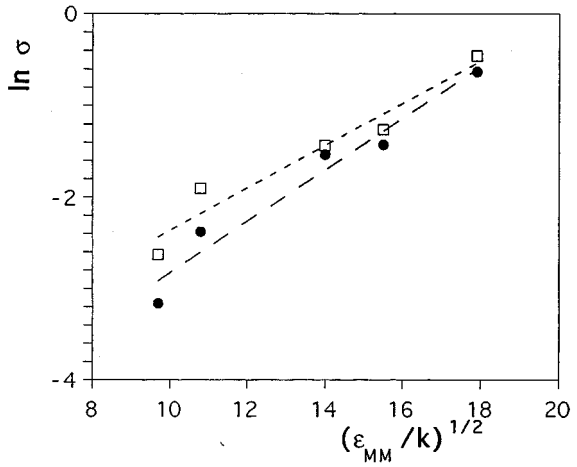

FIG. 8. Plot of the logarithm of the cross section for the collisional quenching removal of four vibronic states within NCO[$\tilde{X}(0n^i0)$] vs the well depth of pairs of reactants for various simple molecules. The straight lines shown are the least-squares best fit for two of the states where the slopes of such plots yield the well depth for the appropriate vibronic states of NCO in the Parmenter–Seaver approximation (see text for table of data).

slopes of the linear plots given in Fig. 8, the following well depths are derived for the vibronic states of NCO:

$$\text{NCO}\ \ \mu^2\Sigma^+(01^00)\quad 90\pm 18\ \ K^{1/2},$$

$$\text{NCO}\ \ ^2\Delta_{5/2}(01^20)\quad 99\pm 20\ \ K^{1/2},$$

$$\text{NCO}\ \ ^2\Pi_{3/2,1/2}(02^10)\quad 87\pm 18\ \ K^{1/2},$$

$$\text{NCO}\ \ ^2\Phi_{7/2}(02^30)\quad 71\pm 14\ \ K^{1/2}.$$

The well depths of the vibronic states of NCO are seen to be much higher than those of the collision partners, as is reasonable to expect, however, the depths are of the same order of magnitude within the estimated errors for the experimental data.

The analysis and rationalization of the present results can also be carried out in terms of a multipolar attractive forces model, also used when considering other relaxation processes in collision-induced, spin-forbidden transitions, intersystem crossing and in magnetic quenching in small polyatomic molecules.[76–80] In this model, vibronic relaxation is assumed to take place in two steps. The appropriate vibronic state of NCO is captured on collision with the quenching molecule (M). The energy is then redistributed within the complex, finally resulting in a dissociative decay mode. The basic assumption of the model is that the form of the collision intermediate is determined by a statistical density of states for some critical configuration. In this case, the cross section for vibronic relaxation, σ_{vr}, is related to the capture cross section, σ_{cap}, by the form

$$\sigma_{\text{vr}}(E)=P_{\text{vr}}(E)\cdot\sigma_{\text{cap}}(E),$$

where $P_{\text{vr}}(E)$ is the probability for the nonradiative decay of the collision complex with relative kinetic energy E. The value of $P_{\text{vr}}(E)$ depends on the unknown intramolecular dynamics of the complex and is assumed to be constant (unity) so that a correlation exist between the experimental and the capture cross sections. The capture cross section is computed by assuming an ''effective'' intermolecular potential, $V_{\text{eff}}(r)$, for the collision pair given as the sum of a centrifugal term, $L^2/2\mu r^2$, and the attractive intermolecular potential expressed in terms of electric multipoles at a distance r,

$$V_{\text{eff}}=L^2/2\mu r^2-C_3/r^3-C_4/r^4-C_6/r^6-C_6'/r^6,$$

where C_n are multipolar contributions described by well established general expressions.[80] These contributions are multipole orientation dependent and considered to assume the maximum value.[75] The capture radius $r^{\#}$ or capture impact parameter, b_{cap}, corresponds to the value at the maximum of the effective potential, i.e., $dV_{\text{eff}}/dr=0$, where the relative kinetic energy of the colliding species is $E\sim V_{\text{eff}}(r^{\#})$. The capture impact parameter or its equivalent, the capture cross section $\sigma_{\text{cap}}=\pi b_{\text{cap}}$, yields the upper limit for the thermal collision rate constant and its related cross section.

Data and computations carried out on the system based on the multipolar attractive forces model are summarized in Table III. Cross sections have been computed from data for the ground NCO state assuming no changes in the multipoles with the vibrational state. As shown in Fig. 9 ($\sigma_{Q,M}$ vs σ_{col}, Table III), the possible slopes, $P(E)$, are very small and increase slightly for near resonant $V-V$ energy transfer. The slope or probability that a given complex will lead to quenching, indicates a very low yield for the $V-T$ process, increasing only slightly for the more dominant $V-V$ process. In both cases the value of $P(E)$ is several orders of magni-

TABLE III. Data used for the calculation of the collision complex model of NCO[$X(000)$] with simple molecules and computed cross sections. The data were taken from Crosley *et al.* (Refs. 77, 78) except those for SO_2 that were taken from Ref. 76 and for NCO, computed with the standard program GAUSSIAN 92 using a basis MP4/6-31G**//MP2/6-31G**.

	σ_{col} (Å^2)	μ_M Debyes	αM Å^3)	Q_M (D A)	I.P. (eV)	$\langle\sigma_{QM}\rangle$/Å^2 (01^00)	(01^20)	(02^10)	(02^30)
N_2	100	0	−1.52	1.77	15.58			0.045	
N_2O	132	0.166	−3.0	3.00	12.89			0.21	
NO	106	0.153	−1.8	1.74	9.25			1.9	
O_2	87	0	−0.39	1.60	12.06			0.083	
CO_2	125	0	−4.3	2.63	13.77			0.21	
SO_2	235	1.63	−7.68	3.89	12.30			0.56	
NCO		0.83	−5.09	6.17	13.16				

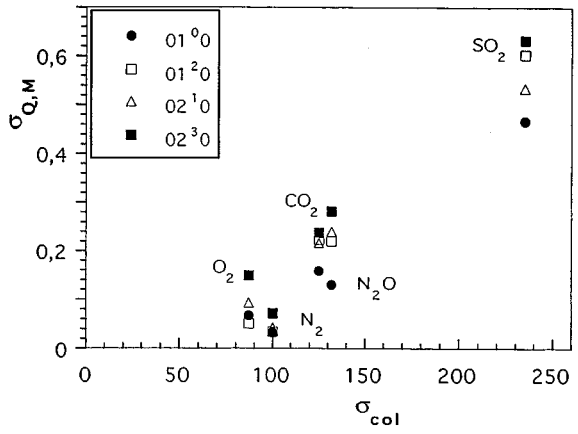

FIG. 9. Correlation between the experimental $\langle \sigma_{Q,M}/\text{Å}^2 \rangle$ and calculated $\langle \sigma_{\text{col}}/\text{Å}^2 \rangle$ quenching cross sections for the collisional removal of NCO($0n0$) involving ($V-V$) and ($V-T$) energy transfer with simple molecules using a multipole attractive force model in the collisional complex assuming no variation in the multipoles with vibrational state.

tude smaller than unity. Other rate constants, even within this already complex system involving NCO, and vibronic levels of other polyatomic molecules, would facilitate the development of a more detailed picture of the correlation between the quenching cross sections and the multipole attractive forces model.

ACKNOWLEDGMENTS

We gratefully acknowledge support of this work by the DGICYT and the Universidad del País Vasco through Grants Nos. PB91-0444 and 039.310-EB 039/92. J.A.F. thanks the GV for a Research Studentship. We also thank Professor A. D. Buckingham F.R.S. for helpful discussions.

[1] I. W. M. Smith, *Kinetics and Dynamics of Elementary Gas Reactions* (Butterworths, London, 1980).
[2] (a) R. J. Donovan and D. Husain, Chem. Rev. **70**, 489 (1970); (b) D. Husain, Ber. Bunsenges. Phys. Chem. **81**, 168 (1977).
[3] G. Herzberg *Molecular Spectra and Molecular Structure. I. Spectra of Diatomic Molecules* (van Nostrand, New York, 1950).
[4] G. Herzberg *The Spectra and Structures of Simple Free Radicals* (Dover, New York, 1988).
[5] J. M. Hollas, *High Resolution Spectroscopy* (Butterworths, London, 1982).
[6] R. Renner, Z. Phys. **92**, 172 (1934); (b) E. Hirota, *High-Resolution Spectroscopy of Transient Molecules* (Springer, Berlin, 1985).
[7] R. N. Dixon, Philos. Trans. R. Soc. London, Ser. A **252**, 165 (1960).
[8] R. N. Dixon, Can. J. Phys. **38**, 10 (1960).
[9] A. Carrington, A. R. Fabris, B. J. Howard, and N. J. D. Lucas, Mol. Phys. **20**, 961 (1971).
[10] P. S. H. Bolman, J. M. Brown, A. Carrington, I. Kopp, and D. A. Ramsay, Proc. R. Soc. London, Ser. A **343**, 17 (1975).
[11] D. R. Woodward, D. A. Fletcher, and J. M. Brown. Mol. Phys. **62**, 453 (1987).
[12] D. R. Woodward, D. A. Fletcher, and J. M. Brown, Mol. Phys. **68**, 261 (1989).
[13] C. E. Barnes, J. M. Brown, A. D. Fackerell, and T. J. Sears, J. Mol. Spectrosc. **92**, 485 (1982).
[14] R. Bruggeman, M. Petri, H. Fisher, D. Mauer, D. Reinert, and W. Urban, Appl. Phys. B **48**, 105 (1989).
[15] J. Werner, W. Seebass, M. Koch, R. F. Curl, W. Urban, and J. M. Brown, Mol. Phys. **56**, 453 (1985).
[16] K. N. Wong, W. R. Anderson, A. J. Kotlar, and J. A. Vanderhoff, J. Chem. Phys. **81**, 2970 (1984).
[17] R. A. Copeland and D. R. Crosley, Can. J. Phys. **62**, 1488 (1984).
[18] D. Patel-Misra, D. G. Sauder, and P. J. Dagdigian, J. Chem. Phys. **93**, 5448 (1990).
[19] D. Patel-Misra, D. G. Sauder, and P. J. Dagdigian, J. Chem. Phys. **95**, 2222 (1991).
[20] M. Wu, F. J. Northrup, and T. J. Sears, J. Chem. Phys. **97**, 4583 (1992).
[21] F. J. Northrup, M. Wu, and T. J. Sears, J. Chem. Phys. **96**, 7218 (1992).
[22] P. J. Dagdigian, M. H. Alexander, and K. Liu, J. Chem. Phys. **91**, 839 (1989).
[23] E. A. Andreev, S. Y. Umansky, and A. A. Zembekov, Chem. Phys. Lett. **18**, 567 (1973).
[24] Ch. Zhurt, L. Zuhlicke, and S. Y. Umansky, Chem. Phys. Lett. **111**, 408 (1984).
[25] Ch. Zhurt, L. Zuchlicke, and S. Y. Umansky, Chem. Phys. **105**, 15 (1986).
[26] E. E. Nikitin, Opt. Spektrosk. **9**, 16 (1960).
[27] C. J. Astbury, G. Hancock, and K. G. McKendrick, J. Chem. Soc. Faraday Trans. **89**, 405 (1993).
[28] K. G. McKendrick, Ph.D. thesis, University of Oxford, 1985; G. Hancock and K. G. McKendrick, Chem. Phys. Lett. **127**, 125 (1986); J. L. Cookson, G. Hancock, and K. G. McKendrick, Ber. Bunsen ges. Phys. Chem. **89**, 335 (1985).
[29] F. Lepoutre, G. Louis, and H. Manceau, Chem. Phys. Lett. **48**, 509 (1977).
[30] F. Lepoutre, G. Louis, and J. Taine, J. Chem. Phys. **70**, 2225 (1979).
[31] S. Lunt, C. T. Wickman-Jones, and C. J. S. M. Simpson, Chem. Phys. Lett. **115**, 60 (1985).
[32] C. T. Wickman-Jones, C. J. S. M. Simpson, and D. C. Clary, Chem. Phys. **117**, 9 (1987).
[33] M. L. Mandich and G. W. Flynn, J. Chem. Phys. **73**, 3679 (1980).
[34] N. J. G. Smith, C. C. Davis, and I. W. M. Smith, J. Chem. Phys. **80**, 6122 (1984).
[35] M. Rebelo da Silva, M. H. Vasconcelos, F. Lepoutre, and M. Y. Perrin, Chem. Phys. Lett. **91**, 135 (1982).
[36] B. D. Cannon and I. W. M. Smith, Chem. Phys. **83**, 429 (1984).
[37] R. N. Schwartz, Z. I. Slawsky, and K. F. Herzfeld, J. Chem. Phys. **20**, 1591 (1952).
[38] R. N. Schwartz and K. F. Herzfeld, J. Chem. Phys. **22**, 767 (1954).
[39] D. C. Clary, Chem. Phys. **65**, 247 (1982).
[40] D. C. Clary, J. Phys. Chem. **91**, 1718 (1987).
[41] A. J. Banks and D. C. Clary, J. Chem. Phys. **86**, 802 (1987).
[42] K. Lin, R. G. McDonnald, and A. F. Wagner, Int. Rev. Phys. Chem. **9**, 187 (1990).
[43] R. G. McDonnald and K. Lin, J. Chem. Phys. **95**, 9630 (1991).
[44] R. G. McDonnald and K. Lin, J. Phys. Chem. **97**, 978 (1992).
[45] L.-H. Lai, Y.-H. Chiu, and K. Liu, J. Chem. Phys. **103**, 8492 (1992).
[46] R. A. Perry, J. Chem. Phys. **82**, 5485 (1985).
[47] B. Atakan and J. Wolfrum, Chem. Phys. Lett. **178**, 157 (1991).
[48] W. F. Cooper, J. Park, and J. F. Hershberger, J. Phys. Chem. **97**, 3283 (1993); W. F. Cooper and J. F. Hershberger, *ibid*. **96**, 771 (1992).
[49] Y. Y. You and N. S. Wang, J. Chin. Chem. Soc. **40**, 337 (1993).
[50] J. Park and J. F. Hershberger, J. Phys. Chem. **97**, 13 647 (1993); Chem. Phys. Lett. **218**, 537 (1994).
[51] A. Schuck, H. R. Volpp, and J. Wolfrum, Combust. Flame **99**, 491 (1994).
[52] K. H. Becker, R. Kurtenbach, and P. Wiesen, J. Phys. Chem. **99**, 5986 (1995); K. H. Becker, R. Kurtenbach, F. Schmidt, and P. Wiesen, Chem. Phys. Lett. **235**, 230 (1995).
[53] Y. W. Chang and N. S. Wang, Chem. Phys. **200**, 431 (1995); D. Y. Juang, J. S. Lee, and N. S. Wang, Int. J. Chem. Kinet. **27**, 1111 (1995).
[54] A. Ortíz de Zárate, R. Martínez, M. N. Sánchez Rayo, F. Castaño, and G. Hancock, J. Chem. Soc. Faraday Trans. **88**, 535 (1992).
[55] A. Ortíz de Zárate, F. Castaño, J. A. Fernández, R. Martinez, M. N. Sánchez Rayo, and G. Hancock, Chem. Phys. Lett. **188**, 265 (1992).
[56] J. A. Fernández, A. Ortíz de Zárate, M. N. Sánchez Rayo, and F. Castaño, Laser Chem. **12**, 43 (1992).
[57] J. A. Fernández, R. Martínez, M. N. Sánchez Rayo, and F. Castaño, J. Phys. Chem. **100**, 12 305 (1996).
[58] J. A. Fernandez, Ph.D. thesis, Universidad del Pais Vasco, 1995.
[59] D. W. Cullin, L. Yu, J. M. Willianson, M. S. Platz, and T. A. Miller, J. Phys. Chem. **94**, 3387 (1990).
[60] D. W. Cullin, N. Soundararajan, M. S. Platz, and T. A. Miller, J. Phys. Chem. **94**, 8890 (1990).

[61] S. E. Bialkowski, D. S. King, and J. C. Stephenson, J. Chem. Phys. **70**, 4010 (1979).
[62] D. L. Akins, D. S. King, and J. C. Stephenson, Chem. Phys. Lett. **65**, 257 (1979).
[63] J. C. Stephenson and D. S. King, J. Chem. Phys. **70**, 4496 (1979).
[64] S. E. Bialkowski, D. S. King, and J. C. Stephenson, J. Chem. Phys. **72**, 1156 (1980).
[65] J. C. Stephenson, S. E. Bialkowski, and D. S. King, J. Chem. Phys. **72**, 1161 (1980).
[66] D. S. King, Adv. Chem. Phys. Dynam. Excited State **L**, 105 (1982).
[67] J. C. Stephenson and D. S. King, J. Chem. Phys. **74**, 1867 (1983).
[68] A. C. G. Mitchell and M. W. Zemansky, *Resonance Radiation and Excited Atoms* (Cambridge University, Cambridge, 1971).
[69] F. Beitia, F. Castaño, and D. Husain, J. Chem. Soc. Faraday Trans. **86**, 795 (1990).
[70] F. Beitia, F. Castaño, M. N. Sánchez Rayo, R. Martinez, L. Santos, and D. Husain, J. Chem. Soc. Faraday Trans. **87**, 1503 (1991).
[71] D. Y. Juang, J. S. Lee, and N. S. Wang, Int. J. Chem. Kinet. **27**, 1111 (1995).
[72] K. H. Becker, R. Kurtenbach, and F. Schmidt, in 14th International Symposium on Gas Kinetics (Book of Abstracts), Leeds, United Kingdom, 1996, paper F4 (unpublished).
[73] J. D. Mertens, A. J. Dean and R. K. Hanson, *Twenty-Fourth Symposium (International) on Combustion* (The Combustion Institute, Pittsburgh, PA 1992), p. 701.
[74] J. D. Mertens, A. J. Dean, and R. K. Hanson, in Proceedings of the 24th International Symposium on Combustion, 1992, 701 (unpublished).
[75] H.-M. Lin, M. Seaver, K. Y. Tang, A. E. W. Tang, and C. S. Parmenter, J. Chem. Phys. **71**, 5442 (1979).
[76] C. S. Parmenter and M. Seaver, J. Chem. Phys. **70**, 5458 (1979).
[77] D. L. Holterman, E. K. C. Lee, and R. Nanes, J. Chem. Phys. **77**, 5327 (1982).
[78] P. W. Fairchild, G. P. Smith, and D. R. Crosley, J. Chem. Phys. **79**, 1795 (1983).
[79] R. A. Copeland, M. J. Dyer, and D. R. Crosley, J. Chem. Phys. **82**, 4022 (1985).
[80] I. García-Moreno, J. M. Figuera, M. Castillejo, and J. C. Rodríguez, J. Phys. Chem. **97**, 8414 (1994).
[81] J. O. Hirschfelder, C. F. Curtiss, and R. B. Bird, *Molecular Theory of Gases and Liquids* (Wiley, New York, 1954).